RSC Advances

PAPER

View Article Online
View Journal | View Issue

Cite this: *RSC Adv.*, 2015, **5**, 38591

An investigation on single crystal growth, structural, thermal and optical properties of a series of organic D–π–A push–pull materials†

Vinod Kumar Gupta and Ram Adhar Singh*

We present the large single crystal growth of a series of donor–π–acceptor (D–π–A) push–pull chromophores; 4-*N*,*N*-dimethylamino-β-nitrostyrene (**1**), 2-(4-(dimethylamino)benzylidene)malononitrile (**2**), ethyl 2-cyano-3-(4-(dimethylamino)phenyl)acrylate (**3**) and methyl 2-cyano-3-(4-(dimethylamino) phenyl)acrylate (**4**). Single crystals with good optical transparency were grown from a mixed organic solvent (1 : 1 acetone–methanol) applying slow evaporation techniques, and crystal dimensions up to 17 × 4 × 1 mm^3 has been successfully achieved in the case of chromophore **4**. A single crystal X-ray diffraction study revealed that two (**3** and **4**) of them belong to the triclinic crystal system with space group $P\bar{1}$, while **1** and **2** crystallize in orthorhombic and monoclinic crystal systems with space groups *Pbca* and $P2_1$, respectively. The packing in all the chromophores (except **2**) is stabilized by C–H···π interaction. Thermal analysis shows higher thermal stability for **2** (T_d = 354 °C), **3** (T_d = 365 °C) and **4** (T_d = 330 °C) than **1** (T_d = 240 °C). The thermodynamic and kinetic parameters, such as heat and entropy of fusion, and activation energy have been determined by exploiting DSC and TGA data, respectively. A Lippert–Mataga plot reflects the highest change in dipole moment on excitation from ground state to excited state for chromophore **3** (4.80 D) followed by **4** (4.45 D), **2** (3.59 D) and **1** (3.17 D). We also report the quantum yield of all the chromophores in different organic solvents. In acetonitrile, it is 0.007, 0.014, 0.023 and 0.019 for chromophores **1**, **2**, **3** and **4**; respectively. These studies indicate the potential opto-electronic application of these push–pull chromophores.

Received 19th March 2015
Accepted 21st April 2015

DOI: 10.1039/c5ra04907e

www.rsc.org/advances

1. Introduction

Molecular design and synthesis of organic charge transfer (OCT) materials have received great scientific attention because of their widespread application in light-emitting diodes,[1] fluorescent dyes,[2] nonlinear optics[3] and optoelectronic devices.[4] Donor–π–acceptor (D–π–A) type chromophores are the simplest example in this series.[5] Such types of π-conjugated molecule have an electron-donor functional group (D) at one end and an electron-acceptor functional group (A) at other end, and exhibit intramolecular charge transfer (ICT) from donor to acceptor.[1,6,7] The advantage of such low energy ICT absorptions with much intensity is that they appear in the region of visible to near infrared (NIR), which are in high demand for various optical applications such as OLEDs. In CT molecules, the redistribution of electronic charge occurs under the application of an electric field through π-conjugation. In the past, several D–π–A systems with different π-bridge and varying substituents (donors and acceptors) have been synthesized and their material properties have been studied experimentally and theoretically, in order to establish the structure–property relationship.[8–10]

Furthermore, there are two main forms in which organic ICT materials can be isolated: polymers and single crystals. Among them, single crystals are the most attractive materials because of their typically large hyperpolarizability, high packing densities, and superior long-term orientational and photochemical stabilities as well as their better optical quality compared to polymeric materials.[11,12] But for practical applications, bulk single crystals with appropriate size and high optical quality are required.[13,14] However, the growth of bulk single crystal of such charge transfer molecules still remain a big challenge.[15,16] This is because of their lower solubility in suitable organic solvent, quick nucleation during cooling/evaporation (in the case of solution growth) and decomposition just after melting during melt growth. Thus the main goal is to synthesize the CT material with better thermal stability and to improve the crystal quality by optimizing the growth conditions. Also, there are several materials in literature

Department of Chemistry, Centre of Advanced Study, Faculty of Science, Banaras Hindu University, Varanasi-221 005, India. E-mail: prrasingh@gmail.com

† Electronic supplementary information (ESI) available: Copies of NMR spectra (^1H and ^{13}C) for the chromophores **1–4**. Crystallographic data in CIF format for **1**, **2**, **3** and **4**. Plots of $1/T$ *versus* ln N_s. A comparative detail of bond lengths and bond angles. View of C–H···π interactions. Thermal activation energy plots. The UV-Vis absorption and fluorescence spectra in different solvents. Lippert–Mataga plots. CCDC 1044113, 1044114, 1020677 and 1020678. For ESI and crystallographic data in CIF or other electronic format see DOI: 10.1039/c5ra04907e

whose large single crystal growth, thermal and material properties have been explored few years after their synthesis. Polyene and stilbazolium crystals[17–19] are benchmark examples of such materials whose single crystal growth and material properties have been widely investigated in last two decades. Therefore, the large single crystal growth and exploration of material properties of earlier reported materials has equal importance as the synthesis of new materials. In this paper, we report the large single crystal growth of 4-*N*,*N*-dimethylamino-β-nitrostyrene (**1**), 2-(4-(dimethylamino)benzylidene)-malononitrile (**2**), ethyl 2-cyano-3-(4-(dimethylamino)phenyl)-acrylate (**3**) and methyl 2-cyano-3-(4-(dimethylamino)phenyl)-acrylate (**4**) by solution growth technique. To the best of our knowledge, no reports have been found related to large single crystal growth, thermal and optical properties of these materials to till date; however their syntheses have been reported earlier.[20–22] The grown single crystals were structurally characterized for FT-NMR and single crystal X-ray diffraction. Solubility of all the materials in a mixed organic solvent (1 : 1 acetone–methanol) has been measured in different range of temperature and various thermodynamic parameters have been calculated for different solute/solvent systems. Differential scanning calorimetry (DSC) and thermo gravimetric-differential thermal analysis (TG-DTA) have been performed to investigate their thermal properties. The UV-Vis absorption and fluorescence spectra have also been recorded in different organic solvents with varying polarity and the quantum yields reported. We also discuss the Lippert–Mataga plots for all the chromophores and the change in dipole moment.

2. Experimental

2.1. Materials and purification

4-*N*,*N*-Dimethylaminobenzaldehyde (Avra Chemical Pvt Ltd) was recrystallized from methanol before used. Ethyl cyanoacetate and methyl cyanoacetate were purchased from Spectrochem Pvt Ltd, while malononitrile, nitromethane and ammonium acetate were received from S d Fine-Chem Ltd. All these chemicals were used as received. 1,8-Diazabicyclo[5.4.0]-undec-7-ene (DBU) (Sigma Aldrich, USA) was also used as received. The solvents were distilled before used.

2.2. Synthesis of chromophores

The synthesis of all the four compounds (**1** to **4**) was performed according to literature procedures.[23]

2.2.1. 4-*N*,*N*-Dimethylamino-β-nitrostyrene (1). 4-*N*,*N*-Dimethylaminobenzaldehyde (10 mmol, 1.49 g) was added to a solution of ammonium acetate (24 mmol, 1.85 g) and nitromethane (60 mmol, 3.25 mL) in AcOH (12 mL) and refluxed for 25 min. The mixture was poured into ice cold water, a red colour precipitate was obtained and filtered. The precipitate was washed properly with water and dried. The dried precipitate was recrystallized from ethanol (yield 1.65 g, 86%). ^{1}H NMR (300 MHz, $CDCl_3$): 7.98 (d, 1H, H–C═C–), 7.41–7.52 (m, 3H, two Ar-H and one –C═C–H), 6.69 (d, 2H, Ar-H), 3.07 (s, 6H, $–CH_3$) ppm.

^{13}C NMR (75 MHz, $CDCl_3$): 140.25, 134.21, 132.15, 131.45, 111.95, 105.83, 40.07 ppm.

2.2.2. 2-(4-(Dimethylamino)benzylidene)malononitrile (2). An equimolar amount of 4-*N*,*N*-dimethylaminobenzaldehyde (1.49 g, 10 mmol) and malononitrile (10 mmol, 0.66 g) mixed thoroughly and then 1 mmol of 1,8-diazabicyclo[5.4.0]undec-7-ene (DBU) (0.15 mL) was added. The reaction mixture was ground in the mortar and pastel for 30 s. The reaction mixture was treated with cold water. The product was filtered, dried, and the crude compounds were recrystallized from a mixture of ethanol and acetone to get the desired compound in pure form (yield 1.90 g, 96%).

^{1}H NMR (300 MHz, $CDCl_3$): 7.81 (d, 2H, Ar-H), 7.44 (s, 1H, H–C═C–), 6.70 (2H, d, Ar-H), 3.14 (s, 6H, $–CH_3$) ppm.

^{13}C NMR (75 MHz, $CDCl_3$): 158.05, 154.22, 133.75, 119.27, 115.93, 114.87, 111.57, 40.03 ppm.

Compounds **3** and **4** were synthesized by similar method.

2.2.3. Ethyl 2-cyano-3-(4-(dimethylamino)phenyl)acrylate (3). 4-*N*,*N*-Dimethylaminobenzaldehyde (10 mmol, 1.49 g), ethyl cyanoacetate (10 mmol, 1.06 mL), DBU (1 mmol, 0.15 mL), grinding time 60 s (yield 2.20 g, 90%).

^{1}H NMR (300 MHz, $CDCl_3$): 8.07 (s, 1H, H–C═C–), 7.94 (d, 2H, Ar-H), 6.70 (d, 2H, Ar-H), 4.36 (q, 2H, $–CH_2–$), 3.11 (s, 6H, $–CH_3$), 1.39 (t, 3H, $–CH_3$) ppm.

^{13}C NMR (75 MHz, $CDCl_3$): 164.24, 154.45, 153.52, 133.10, 119.34, 117.53, 111.45, 94.01, 61.84, 39.97, 14.26 ppm.

2.2.4. Methyl 2-cyano-3-(4-(dimethylamino)phenyl)acrylate (4). 4-*N*,*N*-Dimethylaminobenzaldehyde (10 mmol, 1.49 g), methyl cyanoacetate (10 mmol, 0.88 mL), DBU (1 mmol, 0.15 mL), grinding time 60 s (yield 2.10 g, 91%).

^{1}H NMR (300 MHz, $CDCl_3$): 8.07 (s, 1H, H–C═C–), 7.95 (d, 2H, Ar-H), 6.70 (d, 2H, Ar-H), 3.11 (s, 6H, $–CH_3$), 3.88 (s, 3H, $–CH_3$) ppm.

^{13}C NMR (75 MHz, $CDCl_3$): 164.76, 154.72, 153.63, 134.08, 119.31, 117.52, 111.48, 93.52, 52.76, 39.99 ppm.

2.3. Measurement and characterization

All the NMR spectra were recorded on a FTNMR-JEOL AL300 spectrometer using $CDCl_3$ as a solvent. The single crystal of all the chromophores were grown from the saturated solution of acetone–methanol mixed solvent (1 : 1 by weight) at room temperature by slow evaporation technique. X-ray diffraction data of single crystals were collected using the Xcalibur oxford CCD diffractometer. Structure solution and refinement were carried out utilizing SHELXS and SHLEXL-97. DSC experiment was performed using Mettler TA 4000 machine under nitrogen atmosphere with a heating rate of 10 °C min^{-1}. However, thermo gravimetric-differential thermal analysis (TG-DTA) was performed on a NETZSCH, STA 409 PC analyzer under a nitrogen atmosphere with a heating rate of 10 °C min^{-1} from room temperature to 450 °C. UV-Vis absorption spectra were acquired using a Shimadzu UV-1700 model. Fluorescence spectra were obtained using a JY Horiba fluorescence spectrophotometer. Fluorescence quantum yield was determined by using anthracene as the reference.

3. Results and discussion

3.1. Solubility measurement

The knowledge of solubility of a solute in a particular solvent provides information about the growth conditions and is useful for the thermodynamic analysis of solute–solvent interactions. Solubility analysis of chromophores **1–4** was carried out in acetone and methanol. It has been found that the solubility of all the chromophores is very low in methanol while in acetone it was good. However, due to low boiling point and fast evaporation of acetone it was difficult to get large single crystals with good optical quality. Therefore, we have checked the solubility in various proportions of acetone–methanol. In 1 : 2 mixture of acetone–methanol, the solubility was quite low (Table S1†) to get a large size crystal. However, we avoided the major proportion of acetone because of faster evaporation. That is why we have not carried out solubility in 2 : 1 acetone–methanol mixed solvent. The solubility in 1 : 1 mixture of acetone–methanol was found to be good and therefore chosen for solubility measurement and single crystal growth of chromophores. The solubility curves in 1 : 1 acetone–methanol (by weight) for chromophores **1–4** in the different temperature range are shown in Fig. 1.

For comparison, the solubility of all the chromophores at 37.0 °C is reported in Table 1. In the case of chromophores **1**, **2** and **4** the solubility is almost comparable, however in the case of chromophore **3** it increased into large extent. The structures of chromophores **3** and **4** are almost similar with only difference in ester functionality. The chromophore **3** contains an additional –CH2– group and this group may facilitate interaction of chromophore **3** with solvent and thus results increased solubility.

Such type of interaction has been obtained in the crystal packing of chromophore **3**. In all the cases, solubility is high enough to offer a fast growth rate from the solution and to get a large single crystal.

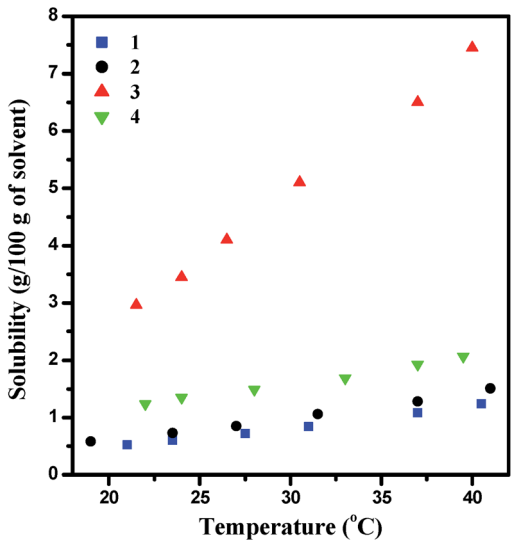

Fig. 1 Solubility curves of chromophores **1**, **2**, **3** and **4** in 1 : 1 acetone–methanol.

The solubility data is described by the van't Hoff equation which correlates the mole fraction of solute (N_s) with change in enthalpy of the solution (ΔH_s) and change in entropy of the solution (ΔS_s), when a solute is dissolve into the solvent/solution.[24]

$$N_s = \exp\left(-\frac{\Delta H_s}{RT} + \frac{\Delta S_s}{R}\right) \quad (1)$$

where T is the absolute temperature and R is the gas constant. The plot of ln N_s against $1/T$ results a straight line (Fig. S9†) from which the values of ΔH_s and ΔS_s can be obtained from slope and intercept of the straight line, respectively. The obtained values of ΔH_s and ΔS_s for different solute (chromophore)/solvent systems are tabulated in Table 1. The values of ΔH_s and ΔS_s are highest in the case of chromophore **3** which is attributed to the much higher solubility of chromophore **3** into the solvent.

3.2. Crystal growth

The seed crystals of all the chromophores **1–4** were grown from the saturated 1 : 1 acetone–methanol solution by slow evaporation technique.

For this purpose, saturated solutions of chromophores were kept at room temperature for slow evaporation of solvent. After a couple of days, small crystals were harvested and used for seeding process. To grow large single crystals of all the chromophores, seeds were inserted into the solutions which were maintained at room temperature. With the slow evaporation of solvent, nucleation started and large single crystals with different dimensions have been obtained within 10 days. The photographs of the grown single crystals of chromophores are shown in Fig. 2. In the case of chromophore **4**, crystal dimensions of 17 × 4 × 1 mm^3 has been successfully achieved. However, for chromophore **3**, 7 × 6 × 1 mm^3 and for chromophore **1**, 4 × 2 × 1 mm^3 have been obtained. Chromophore **2** showed poor growth characteristics and tiny crystals obtained. This might be due to the poorer crystal packing and lack of C–H···π interaction between the molecules. Plate like morphology has been obtained in the case of chromophores **3** and **4**; however **1** is thick needle-shaped with well-formed crystallographic surfaces.

The correlations of between crystal growth and intermolecular interactions have been discussed in Section 4.1. in detail. Based upon these observations, it may be concluded that in a

Table 1 Solubility, change in heat and entropy of solution

Chromophore	Solubility[a] (g per 100 g of solvent)	ΔH_s (kJ mol^{-1})	ΔS_s (J K^{-1} mol^{-1})
1	1.08	33.6	58.0
2	1.28	32.7	56.5
3	6.5	37.3	82.8
4	1.93	21.8	23.1

[a] Solubility at 37.0 °C in mixed 1 : 1 acetone–methanol (by weight) solvent.

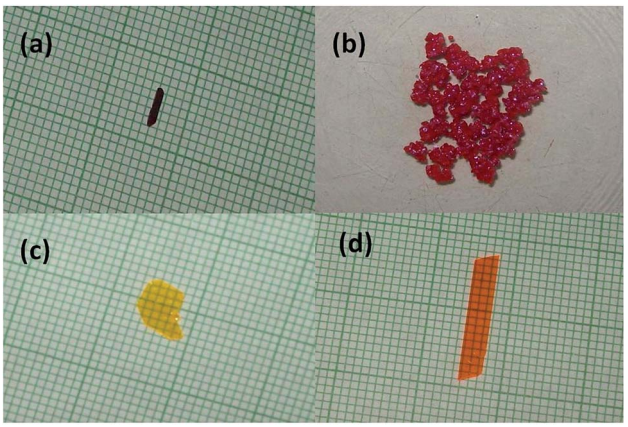

Fig. 2 Grown crystals of (a) chromophore **1**, (b) chromophore **2**, (c) chromophore **3** and (d) chromophore **4** from 1 : 1 acetone–methanol.

particular push–pull system as we increase the strength of electron acceptor groups (as nitrovinyl and dicyanomethylidene in the case of chromophores **1** and **2**, respectively) it will be difficult to get large single crystals with good optical quality.

4. Crystallographic studies

4.1. Crystal structure and packing

The crystal structure of chromophores **1**, **2**, **3** and **4** are reported in Fig. 3. The lattice parameters as well as other crystallographic parameters of the all the crystals are given in Table 2, while the bond angles and bond distances are given in Table S2.† The crystallographic parameters for chromophores **1** and **2** show a good agreement with their previous reported values.[25]

The bond distances and bond angles within the molecules show the usual values, the molecules being nearly perfectly planar. In the crystals, molecules are linked by different types of interactions. In chromophore **1** (C10–H10···O2) and chromophore **2** (C2–H2···N2) only one type of interaction exist. However, chromophore **3** exhibits C11–H11A···N1, C14–H2···C2, C13–H13A···O1 and C5–H5···O1 types of interactions. C13–H13A···C10, C6–H6···O1 and C7–H7···O1 types of interactions have been found in chromophore **4**. A comparative detail of all the interactions, distances and angles are tabulated in Table 3. However, these interactions are represented in Fig. 4. In the case of chromophores **3** and **4**, a view in projection down the *c* axis and down the *b* axis of the crystal packing are shown in Fig. 5 and 6, respectively. Apart from these interactions, the packing in all the crystals (except chromophore **2**) is stabilized by intermolecular C–H···π interaction (Fig. S10–S12†). The centroid to H distance is found to be 4.023, 3.967 and 3.725 Å for chromophores **1**, **3** and **4**, respectively. In the case of chromophore **1**, centroid of other benzene ring also shows interactions with vinyl hydrogens of another molecule. These distances are found to be 3.655 (centroid to α-H) and 3.637 (centroid to β-H) Å.

Furthermore, packing of molecules in a crystal lattice play an important role in single crystal growth of materials. In the case of chromophore **4**, the molecules are connected in head–tail fashion *i.e.*, donor end of one molecule is connected with the acceptor end of second molecule through intermolecular interactions and results in a sheet structure (Fig. 6). In the crystal packing of chromophore **3**, the donor end of one

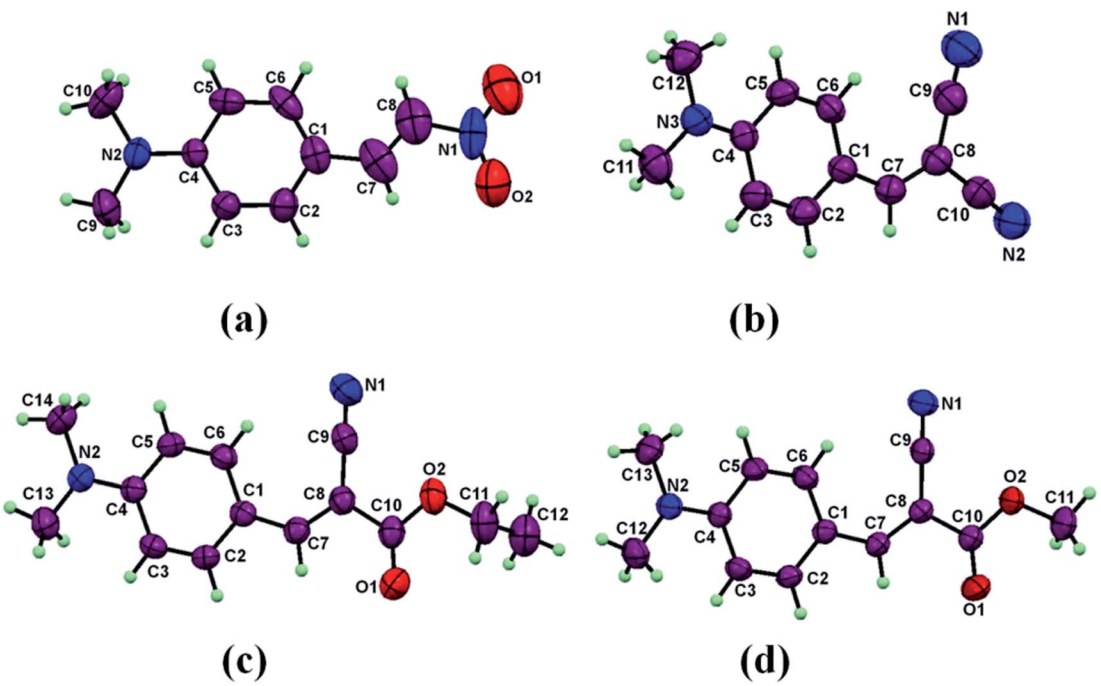

Fig. 3 The molecular structures of (a) chromophore **1**, (b) chromophore **2**, (c) chromophore **3** and (d) chromophore **4** showing displacement ellipsoids at the 50% probability level.

Table 2 Structural parameters for chromophores 1 to 4

	1	2	3	4
Empirical formula	$C_{10}H_{12}N_2O_2$	$C_{12}H_{11}N_3$	$C_{14}H_{16}N_2O_2$	$C_{13}H_{14}N_2O_2$
M_r	192.22	197.24	244.29	230.26
Crystal size (mm)	0.3 × 0.2 × 0.1	0.3 × 0.2 × 0.1	0.4 × 0.3 × 0.2	0.4 × 0.3 × 0.2
Crystal system	Orthorhombic	Monoclinic	Triclinic	Triclinic
Space group	*Pbca*	$P2_1$	$P\bar{1}$	$P\bar{1}$
a [Å]	10.3118(10)	3.9890(5)	7.6022 (17)	7.3225(14)
b [Å]	7.4555(8)	14.0371(12)	8.3944 (18)	7.4824(14)
c [Å]	25.318(3)	9.5430(12)	11.5620(2)	11.5556(16)
α [°]	90	90	106.836(18)	100.830(13)
β [°]	90	100.572(12)	102.222(17)	104.334(14)
γ [°]	90	90	102.304(19)	96.663(15)
V [Å^3]	1946.5(3)	525.28(10)	659.8(2)	593.64(18)
Z	8	2	2	2
D [g cm^{-3}]	1.312	1.247	1.230	1.288
T [K]	293	293	293	293
λ [Å]	0.71073	0.71073	0.71073	0.71073
μ [mm^{-1}]	0.093	0.078	0.083	0.088
F(000)	800	194	260	244
h	−14 to 13	−5 to 4	−10 to 9	−9 to 9
k	−9 to 8	−15 to 17	−11 to 10	−10 to 10
l	−10 to 34	−8 to 12	−15 to 14	−14 to 15
θ range for data collection (°)	3.47 to 29.18	4.58 to 29.14	3.78 to 29.09	3.69 to 29.11
Reflections measured	4854	2036	5025	4303
Reflections unique	2192	1665	3538	2659
Data with $F_o > 2\sigma(F_o)$	1222	946	2017	1818
Parameters refined	127	138	166	154
Final R indices	0.0844	0.0494	0.0473	0.0504
Final wR indices	0.2121	0.0539	0.1177	0.1089
Goodness of fit	0.952	0.878	1.029	1.031
CCDC number	1044113	1044114	1020677	1020678

molecule connect with the acceptor end of second molecule to form a layer and this layer further connect with second layer in head–tail fashion of the molecules. Thus give a 3D-sheet arrangement as shown in Fig. 5. However, in the case of chromophores **1** and **2**, no such arrangements have been found (as discussed above). Thus, in the case of chromophores **3** and **4**, during slow evaporation controlled nucleation will take place and that will grow in such a way to results a large single crystal.

Table 3 Short-contact geometry (Å, °) for chromophores 1 to 4

D–H···A	D–H	H···A	D···A	D–H···A
Chromophore 1				
C10–H10A···O2	0.959	2.580	3.530	170.39
C10–H10B···O2	0.959	2.717	3.668	171.68
Chromophore 2				
C2–H2···N2	0.930	2.673	3.385	133.89
Chromophore 3				
C11–H11A···N1	0.97	2.593	3.503	156.32
C14–H2···C2	0.931	2.894	3.782	160.14
C13–H13A···O1	0.960	2.606	3.542	164.80
C5–H5···O1	0.930	2.672	3.445	141.07
Chromophore 4				
C13–H13A···C10	0.960	2.888	3.533	125.51
C6–H6···O1	0.930	2.506	3.387	158.18
C7–H7···O1	0.930	2.635	3.508	156.75

4.2. Thermal properties

The thermal properties of all the chromophores were studied by TG-DTA and DSC under a nitrogen atmosphere. The obtained

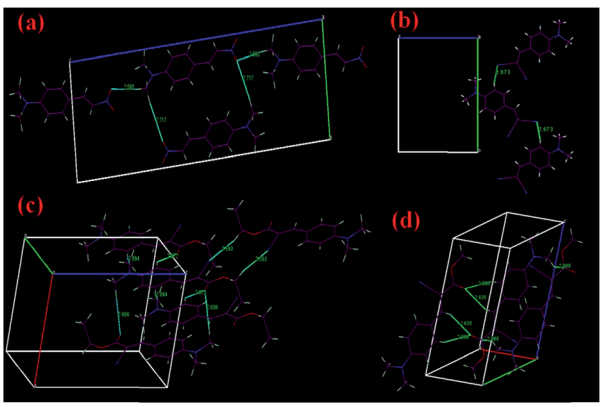

Fig. 4 View of intermolecular interactions in (a) chromophore **1**, (b) chromophore **2**, (c) chromophore **3** and (d) chromophore **4**.

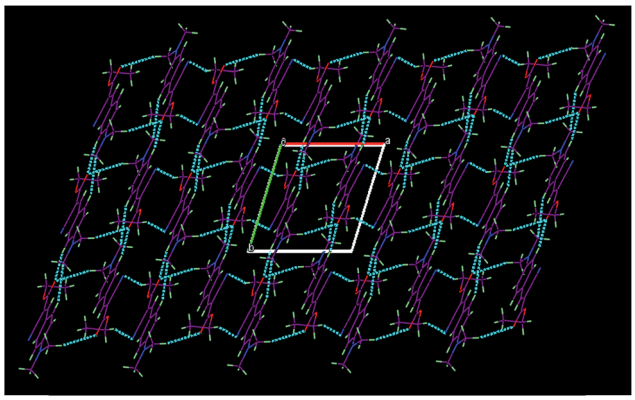

Fig. 5 A view in projection down the *c*-axis of crystal packing in chromophore **3**.

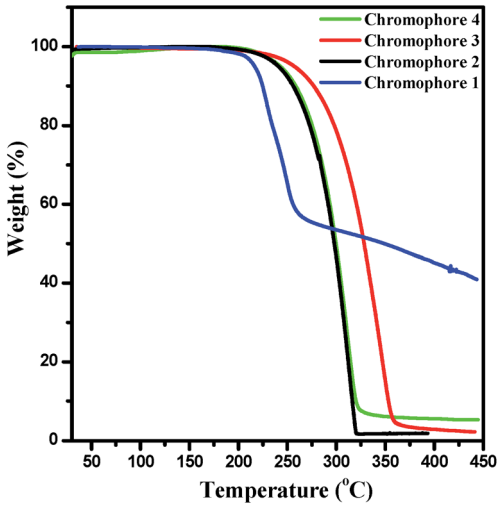

Fig. 7 TGA curve of chromophores **1**, **2**, **3** and **4**.

curves are shown in Fig. 7–9. The TGA data revealed that the chromophores **2**, **3** and **4** showed higher thermal stabilities as compared to **1**. Chromophore **1** showed 43% weight loss in the temperature range 208–261 °C and about 16% in the range of 262–443 °C. In the case of chromophores **2**, **3** and **4** almost similar single step weight losses have been observed. From the TGA data, the amount of carbonized residue (char yield)[26] of **1** has been found (20%) higher than **2**, **3** and **4** with almost complete weight loss. This may be attributed to the presence of entirely different acceptor moiety (nitrovinyl) in the chromophore **1**. DTA curve of all the derivatives reflect two peaks, one in the lower temperature region corresponds to melting temperature and second one represent the decomposition temperature of the materials. The decomposition temperature obtained for chromophores **1** to **4** are 240, 354, 365 and 330 °C, respectively. DSC curves exhibit sharp endothermic peaks which are assigned as melting temperatures of chromophores. Also, the heat of fusion and entropy of fusion values were calculated using DSC data. The heat and entropy of fusion values along with their melting and decomposition temperatures are shown in Table 4.

The activation energy associated with each stage of decomposition is described by the equation:[27]

$$\ln\left[\ln\left(\frac{1}{y}\right)\right] = \left(-\frac{E_a}{R}\right)\frac{1}{T} + \text{Constant} \quad (2)$$

where $y = (W_t - W_\infty)/(W_o - W_\infty)$ is the fraction of the number of initial molecules not yet decomposed, E_a is the activation energy, R is the gas constant, T is the absolute temperature, W_t is the weight at any time t, W_∞ is the weight at infinite time.

A plot of $\ln[\ln(1/y)]$ *vs.* $1/T$ gives an good approximation to a straight line (Fig. S14†) and the activation energy have been calculated using the slope of the straight line. The obtained values of activation energy in the particular decomposition range for all the chromophores are also tabulated in Table 4. The lower activation energy in the case of chromophores **2**, **3** and **4** than chromophore **1** could be attributed to their higher heat liability.

4.3. Optical properties

4.3.1. Absorption spectral study. The electronic absorption spectra of chromophores **1** to **4** have been compared in acetonitrile and shown in Fig. 10. All the chromophores exhibit

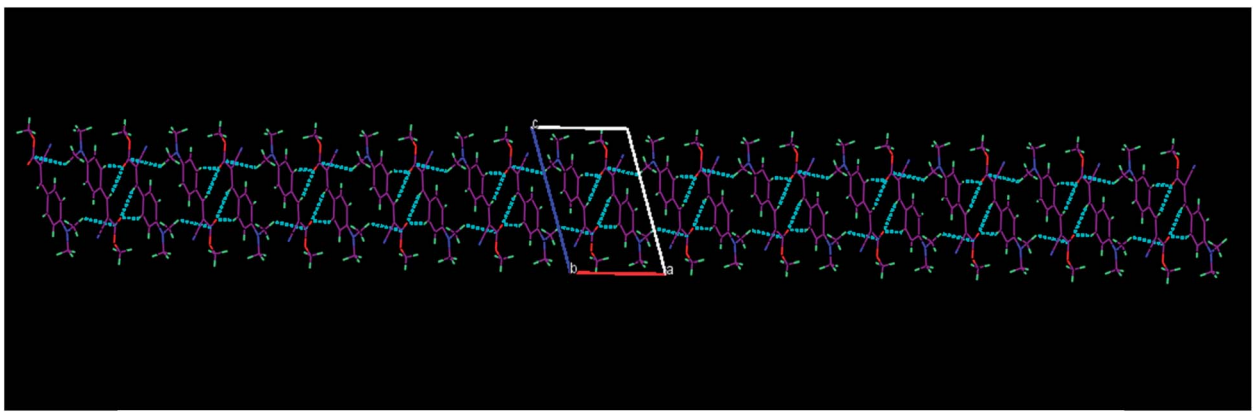

Fig. 6 A view in projection down the *b* axis of the crystal packing in chromophore **4**.

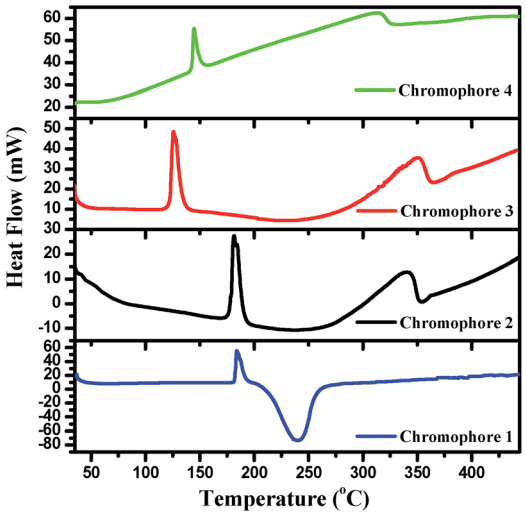

Fig. 8 DTA curve of chromophores 1, 2, 3 and 4.

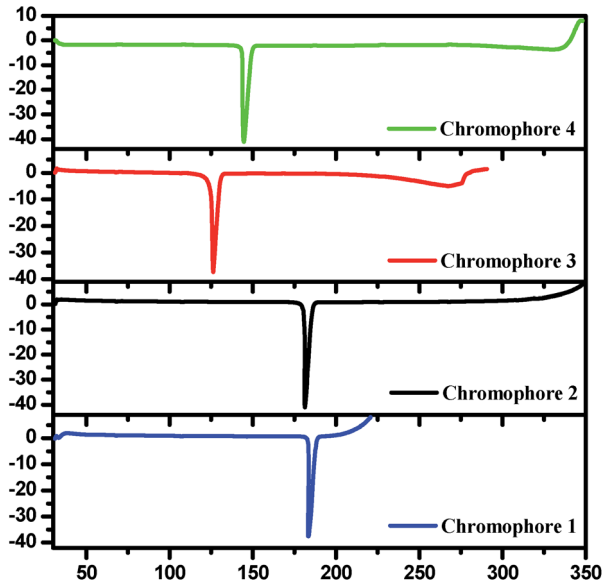

Fig. 9 DSC curve of chromophores 1, 2, 3 and 4.

intense absorption bands in the wavelength region 421 to 439 nm which are characteristic of highly π-conjugated molecules and thus could be attributed to an intramolecular charge transfer (ICT) π–π* transitions. The ICT transitions in chromophores **1** to **4** occurs from the donor *N*,*N*-dimethylamino group to acceptors nitrovinyl, dicyanomethylidene, cyano(ethoxycarbonyl)methylidene and cyano(methoxycarbonyl)methylidene, respectively. A decrease up to 18 nm in λ_{max} value has been observed as we move from chromophore **1** to **4**. This decrease in λ_{max} value could be credited to a decrease in the strength of acceptor group from nitrovinyl to cyano(methoxycarbonyl)methylidene for chromophores **1** to **4**, respectively.

The electronic absorption spectra were also studied in different solvents with varying polarity and found to be sensitive to solvent polarity. In the case of chromophore **1** as the solvent polarity increased from toluene to dimethyl formamide (DMF), the absorption maximum is shifted by 22 nm toward a longer wavelength region. However, for chromophores **2**, **3** and **4** the shifting was found to be 11, 9 and 9 nm, respectively. The electronic absorption spectra in various solvents for all the chromophores are given in Fig. S15.† The λ_{max} values along with their molar extinction coefficient (ε) for all the chromophores are tabulated in Table 5.

4.3.2. Fluorescence spectral studies. Fluorescence spectra of all the chromophores have been recorded in both solution and solid phases using their λ_{max} values as excitation wavelength, and are discussed separately as follows:

4.3.2.1. In solution. All the chromophores exhibit strong fluorescence in acetonitrile solution, except chromophore **1** which shows a weaker emission as reported in Fig. 11.

Strong emission in these chromophores arises from a state which is more polar than the ground state and probably a intramolecular charge-transfer (ICT) state. Like absorption, the fluorescence emission reflects a red shift with increase in solvent polarity from toluene to DMF (Fig. S16†). Also, the fluorescence behaviour is greatly affected by the nature of solvent. Chromophores **2**, **3** and **4** exhibit stronger fluorescence in DMF as compared to other solvent. In toluene, chromophore **1** surprisingly shows very strong emission while in methanol, acetonitrile and DMF its emission is almost negligible. The absence of CT fluorescence in chromophore **1** in polar solvents may be attributed to fluorescence quenching by the rehybridized intramolecular charge transfer (RICT) state.[28]

The change in dipole moment is an important parameter in charge transfer processes and its evaluation is quite useful in designing materials for various optical and nonlinear optical applications. Several methods have been reported to evaluate the change in dipole moment. In this connection, the Lippert–Mataga equation that relates the Stokes shift to the dipole

Table 4 Showing melting temperature, decomposition temperature, heat of fusion, entropy of fusion and thermal activation energy

Chromophore	T_m[a] (°C)	T_d[b] (°C)	ΔH_f (kJ mol^{-1})	ΔS_f (J K^{-1} mol^{-1})	Decomposition range (°C)	E_a[c] (kJ mol^{-1})
1	184.0	240.0	29.83	65.35	208–261	187.75
2	181.0	354.0	31.00	68.24	220–311	146.28
3	126.0	365.0	28.79	72.12	235–360	131.96
4	145.0	330.0	32.14	76.96	225–330	136.50

[a] Melting temperature obtained from DSC. [b] Decomposition temperature obtained from DTA. [c] Activation energy has been calculated using TGA data in the particular decomposition region.

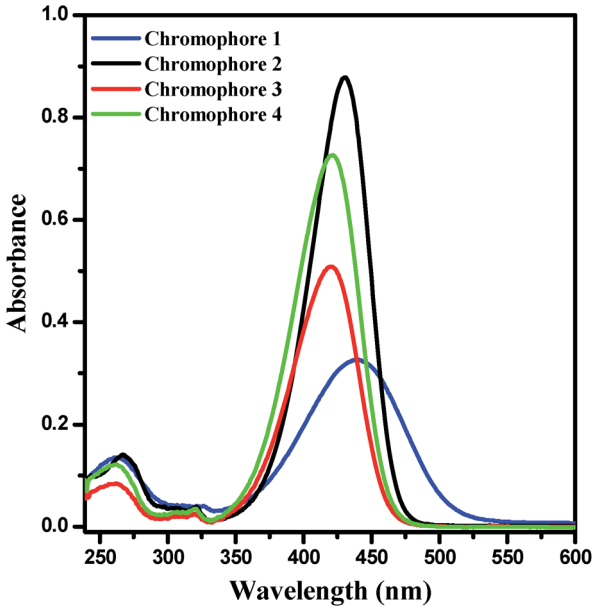

Fig. 10 Absorption spectra of chromophores **1**, **2**, **3** and **4** in acetonitrile with molar concentration 1.0 × 10^{-5} M.

moment of the excited state is a simple and widely used formula as shown in eqn (3):[29,30]

$$\Delta\bar{\upsilon} = \bar{\upsilon}_{\max}^{\text{abs}} - \bar{\upsilon}_{\max}^{\text{emi}} = \frac{2(\mu_e - \mu_g)^2}{hca^3}\Delta f + \text{Constant} \quad (3)$$

In the above equation $(\mu_e - \mu_g)$ = change in dipole moments of the excited and ground state, h = Planck's constant, c = velocity of light, a = Onsager cavity radius of interaction [= $(3M/4\pi dN)^{1/3}$, where d is the density of the solute molecule,

Table 5 Optical properties of chromophores **1** to **4** in different solvents

Compound	Solvent	$\lambda_{\max}^{\text{abs}}$ (nm)	ε (L mol^{-1} cm^{-1})	$\lambda_{\max}^{\text{emi}}$ (nm)	$\Delta\bar{\upsilon}_{\text{st}}$ (cm^{-1})	ϕ_F [a]
1	DMF	447	81 008	557	4418	0.009
1	MeCN	439	32 642	536	4122	0.007
1	MeOH	434	16 305	527	4066	0.010
1	Toluene	425	34 128	503	3649	0.087
2	DMF	437	73 731	487	2349	0.022
2	MeCN	431	87 930	483	2497	0.014
2	MeOH	429	44 622	473	2168	0.014
2	Toluene	426	94 972	460	1735	0.012
3	DMF	427	61 984	485	2801	0.036
3	MeCN	421	50 645	480	2920	0.023
3	MeOH	421	50 613	474	2656	0.018
3	Toluene	418	85 064	455	1945	0.017
4	DMF	427	79 114	485	2800	0.034
4	MeCN	421	72 497	482	3004	0.019
4	MeOH	422	63 131	474	2600	0.018
4	Toluene	418	51 391	456	1994	0.018

[a] Quantum yield of all the chromophores have been calculated using anthracene as a reference (ϕ_F = 0.20 in methanol).[36]

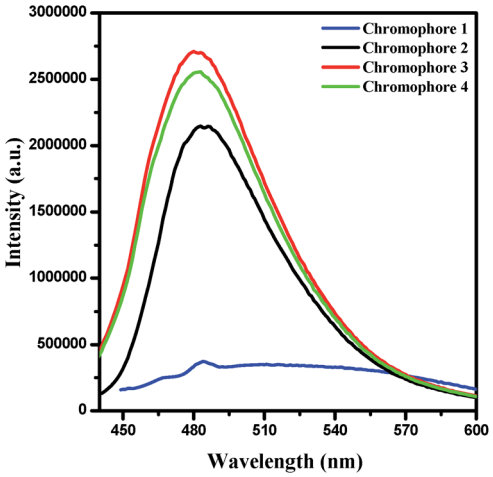

Fig. 11 Fluorescence spectra of chromophores **1**, **2**, **3** and **4** in acetonitrile with molar concentration 1.0 × 10^{-5} M.

M is the molecular weight of solute and N is the Avogadro number] and Δf = Lippert–Mataga solvent polarity parameter and is the function of static dielectric constant ε and the refractive index of the solvent and defined as:[31,32]

$$\Delta f = \left[\frac{(\varepsilon - 1)}{(2\varepsilon + 1)} - \frac{(n^2 - 1)}{(2n^2 + 1)}\right] \quad (4)$$

The plot of solvent polarity function *versus* stokes shift shows a linear variation (Fig. S17†). The change in dipole moments $(\mu_e - \mu_g)$ for all the chromophore have been calculated from the slope of the curve and found to be 3.17, 3.59, 4.80 and 4.45 D for chromophores **1**, **2**, **3** and **4**, respectively. Thus significant change in dipole moment on excitation has been observed. This could be attributed to the presence of a non-classical twisted intramolecular charge transfer (TICT) and increase in planarity on excitation make the molecule more polar as compared to ground state. The change was found to be highest for chromophore **3** and lowest for chromophore **1** while chromophores **2** and **4** showed moderate change. The lowest change in case of chromophore **1** might be due to its ground state is more polar than the ground state of other chromophores.

4.3.2.2. In solid. The recorded solid state fluorescence spectra of all the chromophores differ in their emission behavior compared to that in solution and a pronounced red-shift has been noted. The spectra are shown in Fig. 12.

This could be attributed to the inter-fluorophore interactions in the solid state. Such type of interactions in chromophores has also been proved by the X-ray crystallographic studies. Similar results have been observed for the several luminophores.[33] Chromophores **1** and **2** reflect a single broad emission band at 607.0 and 533.5 nm, respectively. However, in the case of chromophores **3** and **4** dual fluorescence has been observed.

In the case of chromophores **3** and **4** it is assumed that, donor and acceptor groups have a minimum overlap in the CT states and may results in dual fluorescence as reported. Furthermore, this interesting behavior of dual fluorescence in the case of chromophores **3** and **4** may be explained based upon

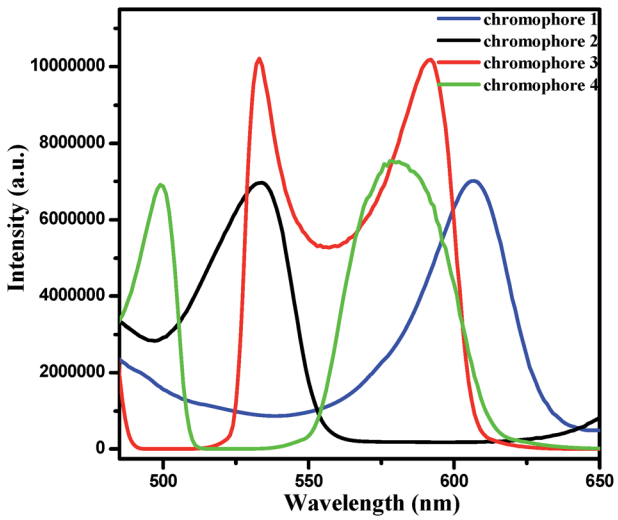

Fig. 12 Fluorescence spectra of chromophores 1, 2, 3 and 4 in solid.

their crystal structure and packing. Chromophores **3** and **4** contain two molecules in their unit cells which are almost parallel to each other [Fig S13(c) and (d)†] and results in 3D-sheet arrangement in crystal lattice (Fig. 5 and 6) as discussed in Section 4.1. Such type of parallel arrangement of molecules has been found in the packing of 4-(diisopropylamino)benzonitrile (DIABN)[34] and responsible for dual fluorescence in solid state.[35] This is because smaller energy gap ΔE(S1, S2) between the two lowest excited singlet states leads to a lowering of barrier for dual fluorescence. However, in the case of chromophore **1** eight molecules are present in unit cell are distributed in four pairs and each pair have the two molecules almost perpendicular to each other [Fig. S13(a)†]. In the case of chromophore **2**, the two molecules in unit cell are distant apart and no such interaction exists [Fig. S13(b)†].

5. Conclusions

We have explored a comparative study about the solubility and large single crystal growth of a series of push–pull chromophores **1** to **4** having dimethylamino group as an electron donor with varying electron acceptors. Chromophores **3** and **4** showed better growth rate and optical quality than chromophores **1** and **2**. Chromophores **2**, **3** and **4** exhibit relatively higher thermal stability with decomposition temperatures more than 300.0 °C. Chromophores **2**, **3** and **4** are highly fluorescent in solution as well in solid state. However, chromophore **1** exhibit strong fluorescence in solid state, and in solution its fluorescent property is solvent dependent (fluoresce only in toluene). All the chromophores possess a significant change in dipole moment upon excitation. Quantum yield of chromophores did not vary drastically with the change in solvent polarity. Thus solubility, crystal quality, thermal and optical properties of charge transfer chromophores is sensitive to the nature of acceptor moiety. These studies give a new direction to give grow large single crystals of push–pull chromophores for various opto-electronic applications.

Acknowledgements

V. K. Gupta is thankful to the University Grant Commission (UGC), New Delhi for the award of BSR meritorious fellowship.

References

1 S. Reineke, *Nat. Photonics*, 2014, **8**, 269–270.
2 R. N. Dsouza, U. Pischel and W. M. Nau, *Chem. Rev.*, 2011, **111**, 7941–7980.
3 Ch. Bosshard, M. Bosch, I. Liakatas, M. Jager and P. Gunter, in *Nonlinear optical effects and materials*, ed. P. Gunter, Springer-Verlag, Berlin, 2000, ch. 3.
4 S. Roquet, A. Cravino, P. Leriche, O. Aleveque, P. Frere and J. Roncali, *J. Am. Chem. Soc.*, 2006, **128**, 3459–3466.
5 M. Klikar, F. Bures, O. Pytela, T. Mikysek, Z. Padelkova, A. Barsella, K. Dorkenood and S. Achelle, *New J. Chem.*, 2013, **37**, 4230–4240.
6 X. Y. Shen, W. Z. Yuan, Y. Liu, Q. Zhao, P. Lu, Y. Ma, I. D. Williams, A. Qin, J. Z. Sun and B. Z. Tang, *J. Phys. Chem. C*, 2012, **116**, 10541–10547.
7 B. Carlotti, A. Spalletti, M. Sindler-Kulykb and F. Elisei, *Phys. Chem. Chem. Phys.*, 2011, **13**, 4519–4528.
8 J. Y. Lee and K. S. Kim, *J. Chem. Phys.*, 2001, **115**, 9484–9489.
9 T. Seidler, K. Stadnicka and B. Champagne, *J. Chem. Theory Comput.*, 2014, **10**, 2114–2124.
10 C. Botta, E. Cariati, G. Cavallo, V. Dichiarante, A. Forni, P. Metrangolo, T. Pilati, G. Resnati, S. Righetto, G. Terraneoc and E. Tordin, *J. Mater. Chem. C*, 2014, **2**, 5275–5279.
11 Z. Yang, M. Jazbinsek, B. Ruiz, S. Aravazhi, V. Gramlich and P. Gunter, *Chem. Mater.*, 2007, **19**, 3512–3518.
12 B. J. Coe, J. A. Harris, I. Asselberghs, K. Wostyn, K. Clays, A. Persoons, B. S. Brunschwig, S. J. Coles, T. Gelbrich, M. E. Light, M. B. Hursthouse and K. Nakatani, *Adv. Funct. Mater.*, 2003, **13**, 347–357.
13 P. J. Kim, M. Jazbinsek and O. P. Kwon, *Cryst. Growth Des.*, 2011, **11**, 3060–3064.
14 P. J. Kim, J. H. Jeong, M. Jazbinsek, S. J. Kwon, H. Yun, J. T. Kim, Y. S. Lee, I. H. Baek, F. Rotermund, P. Gunter and O. P. Kwon, *CrystEngComm*, 2011, **13**, 444–451.
15 O. P. Kwon, B. Ruiz, A. Choubey, L. Mutter, A. Schneider, M. Jazbinsek, V. Gramlich and P. Gunter, *Chem. Mater.*, 2006, **18**, 4049–4405.
16 S. J. Kwon, M. Jazbinsek, O. P. Kwon and P. Gunter, *Cryst. Growth Des.*, 2010, **10**, 1552–1558.
17 (*a*) T. Kolev, Z. Glavcheva, D. Yancheva, M. Schürmann, D. C. Kleb, H. Preut and P. Bleckmann, *Acta Crystallogr., Sect. E: Struct. Rep. Online*, 2001, **57**, o561–o562; (*b*) S. H. Lee, M. J. Koo, M. Jazbinsek and O. P. Kwon, *Cryst. Growth Des.*, 2014, **14**, 6024–6032.
18 (*a*) J. Y. Seo, M. Jazbinsek, E. Y. Choi, S. H. Lee, H. Yun, J. T. Kim, Y. S. Lee and O. P. Kwon, *Cryst. Growth Des.*, 2013, **13**, 1014–1022; (*b*) T. C. Lin, J. M. Cole, A. P. Higginbotham, A. J. Edwards, R. O. Piltz, J. Perez-Moreno, J. Y. Seo, S. C. Lee, K. Clays and O. P. Kwon, *J. Phys. Chem. C*, 2013, **117**, 9416–9430.

19 (*a*) S. R. Marder, J. W. Perry and W. P. Schaefer, *Science*, 1989, **245**, 626–628; (*b*) Z. Yang, S. Aravazhi, A. Schneider, P. Seiler, M. Jazbinsek and P. Gunter, *Adv. Funct. Mater.*, 2005, **15**, 1072–1076.
20 C. Wang and S. Wang, *Synth. Commun.*, 2002, **32**, 3481–3486.
21 M. Saha, S. Roy, S. K. Chaudhuri and S. Bhar, *Green Chem. Lett. Rev.*, 2008, **1**(2), 113–121.
22 G. Kaupp, M. R. N. Jamal and J. Schmeyers, *Tetrahedron*, 2003, **59**, 3753–3760.
23 (*a*) S. Atkinson and P. Meredith, *Synlett*, 2003, **12**, 1853–1855; (*b*) M. Ware, B. Madje, R. K. Pokalwar, G. Kakade and M. Shingare, *Bull. Cat. Soc. India*, 2007, **6**, 104–106.
24 S. J. Kwon, M. Jazbinsek, O. P. Kwon and P. Gunter, *Cryst. Growth Des.*, 2010, **10**(4), 1552–1558.
25 (*a*) L. Hamdellou, O. Hernandezb and J. Meinnel, *Acta Crystallogr., Sect. C: Cryst. Struct. Commun.*, 2006, **62**, o557–o560; (*b*) M. Y. Antipin, T. V. Timofeeva, R. D. Clark, V. N. Nesterov, M. Sanghadasa, T. A. Barr, B. Penn, L. Romero and M. Romero, *J. Phys. Chem. A*, 1998, **102**, 7222–7232.
26 X. Feng, J. Y. Hu, H. Tomiyasu, N. Seto, C. Redshaw, M. R. J. Elsegoodd and T. Yamato, *Org. Biomol. Chem.*, 2013, **11**, 8366–8374.
27 (*a*) A. Broido, *J. Polym. Sci.*, 1969, **7**, 1761–1773; (*b*) M. Tiwari, S. Gupta and R. Prakash, *RSC Adv.*, 2014, **4**, 25675–25682.
28 A. L. Sobolewski, W. Sudholt and W. Domcke, *J. Phys. Chem. A*, 1998, **102**, 2716–2722.
29 (*a*) E. Lippert, *Z. Elektrochem.*, 1957, **61**, 962–975; (*b*) N. Mataga, Y. Kaifu and M. Koizumi, *Bull. Chem. Soc. Jpn.*, 1956, **29**, 465–470.
30 (*a*) N. Mataga, *Bull. Chem. Soc. Jpn.*, 1963, **36**, 654–662; (*b*) A. P. Demchenko, K.-C. Tangb and P.-T. Chou, *Chem. Soc. Rev.*, 2013, **42**, 1379–1408.
31 S. Nad, M. Kumbhakar and H. Pal, *J. Phys. Chem. A*, 2003, **107**, 4808–4816.
32 Z. R. Grabowski and K. Rotkiewicz, *Chem. Rev.*, 2003, **103**, 3899–4031.
33 (*a*) M. D. Allendorf, C. A. Bauer, R. K. Bhakta and R. J. T. Houk, *Chem. Soc. Rev.*, 2009, **38**, 1330–1352; (*b*) J. Cornil, D. A. D. Santos, X. Crispin, R. Silbey and J. L. Bredas, *J. Am. Chem. Soc.*, 1998, **120**, 1289–1299.
34 W. Frey, C. Root, P. Gilch and M. Braun, *Z. Kristallogr. NCS*, 2004, **219**, 291–292.
35 S. I. Druzhinin, A. Demeter and K. A. Zachariasse, *Chem. Phys. Lett.*, 2001, **347**, 421–428.
36 P. Hrdlovic, J. Donovalova, H. Stankovicova and A. Gaplovsky, *Molecules*, 2010, **15**, 8915–8932.

